

# The Effect of F-Actin on the Relay Helix Position of Myosin II, as Revealed by Tryptophan Fluorescence, and Its Implications for Mechanochemical Coupling<sup>†</sup>

Paul B. Conibear,\* András Málnási-Csizmadia,# and Clive R. Bagshaw\*<sup>‡</sup>

Department of Biochemistry, University of Leicester, Leicester LE1 7RH, United Kingdom, and Department of Biochemistry, Eötvös Loránd University, H-1117 Budapest, Pázmány Péter sétány 1/C, Hungary

Received August 3, 2004; Revised Manuscript Received September 20, 2004

**ABSTRACT:** The fluorescence properties of *Dictyostelium discoideum* (*Dd*) myosin II constructs containing a single tryptophan residue have revealed detailed information regarding nucleotide binding and hydrolysis steps. Here we extend these studies to investigate the influence of actin on nucleotide-induced fluorescence transients. The fluorescence from native actin tryptophan residues is not significantly perturbed on binding to myosin, although an apparent signal is detected as a consequence of a light scatter artifact. Actin has a minor effect on the response of W129, located at the entrance to the nucleotide-binding pocket, and reduces the forward rate constants for the isomerization(s) associated with binding of ATP, ATP $\gamma$ S, and ADP by 3-fold or less. The isomerization detected by W129 clearly precedes the dissociation of actin in the case of ADP and ATP $\gamma$ S binding. The fluorescence from the conserved W501 residue, located at the distal end of the relay helix, is very sensitive to the switch 2 and/or lever arm disposition. Consequently, the observed fluorescence emission intensity can be used to estimate the equilibrium constant between the pre- and post-power stroke conformations. Actin modulates this equilibrium by no more than 2-fold in the presence of nucleoside triphosphate. These data have implications for the mechanism of product release and suggest that actin activates another process in the mechanism, such as switch 1 movement and Pi release, rather than influencing the switch 2 equilibrium and lever arm position directly.

Understanding the molecular mechanism of actomyosin-based motors entails relating structural states with kinetically determined states. Prior to the availability of high-resolution structures of the myosin motor domain, tryptophan fluorescence was used as an empirical signal for transient kinetic measurements to define biochemical states (1–4). In light of the crystal structures, this signal can now be interpreted in greater detail (5). In particular, by engineering myosin constructs to contain just one tryptophan, the origin of the signal can be defined specifically. Such an approach has enabled the properties of a conserved tryptophan (W501 in *Dictyostelium discoideum* (*Dd*),<sup>1</sup> W510 in chicken fast skeletal myosin), located at the end of the so-called relay helix, to be partly rationalized in terms of two basic conformations of the myosin motor (6). These conformations, termed the open- and closed-states refer to the position of the switch 2 loop. The switch 2 loop defines the proximal end of the relay helix, whereas W501 is located on a loop at the distal end of the helix. In the open conformation, first

defined in an ADP•BeF<sub>x</sub> complex with the *Dd* myosin II (7), the switch 2 loop was several angstroms away from the putative  $\gamma$ -Pi position occupied by the BeF<sub>x</sub> moiety. In the closed conformation, first defined by the ADP•AlF<sub>4</sub> complex with *Dd* myosin II (7), the switch 2 loop moved in toward the AlF<sub>4</sub>. This movement results in the rotation of the relay helix, but steric clashes with residues at the end of an adjacent  $\beta$ -sheet causes the helix to kink about halfway along its length at residue F487 (Figure 1). The kink amplifies the movement of the distal end of the relay helix (5, 8). Throughout this movement, the converter domain maintains close contact with the distal end of the relay helix and therefore it moves accordingly (9). In turn, the converter domain maintains rigid contact with the C-terminal light chain binding helix and swings through around a 60° angle, so that the latter acts as a lever arm to amplify the initial small movement of switch 2. This mechanism underlies the basis of the lever arm swing from the postpower stroke (lever down) to the prepower stroke (lever up) states. The question remains in the detail as to how actin binding to the myosin head in the prepower stroke state causes it to return to the post stroke position, thereby executing relative movement of the actin and myosin molecules (5, 8).

The conserved tryptophan at the end of the relay helix (*Dd* W501) is ideally placed to report these events (Figure 1). If the switch 2 position and lever arm orientation are tightly coupled via the relay helix, then the fluorescence emission intensity of W501 can be interpreted in terms of the two crystal structures alluded to above. Thus nucleotides that favor the switch 2 open state give a lower fluorescence

<sup>†</sup> This work was supported by the Wellcome Trust, the Biotechnology and Biological Sciences Research Council, the Magyary Zoltán Foundation, the Bekesy fellowship and the European Molecular Biology Organization-Howard Hughes Medical Institute Young Investigators Program to A.M.-C.

\* To whom correspondence should be addressed. Tel: +44 (0)116 252 3454. Fax: +44 (0)116 252 3369. E-mail: crb5@le.ac.uk.

<sup>‡</sup> University of Leicester.

# Eötvös Loránd University.

<sup>1</sup> Abbreviations: A, actin; AMP-PNP, adenosine 5'-( $\beta$ , $\gamma$ -imidotriphosphate); ATP $\gamma$ S, adenosine 5'-O-(3-thiotriphosphate), BeF<sub>x</sub>, beryllium fluoride with undefined stoichiometry; *Dd*, *Dictyostelium discoideum*; M, myosin motor domain. Vi, vanadate.

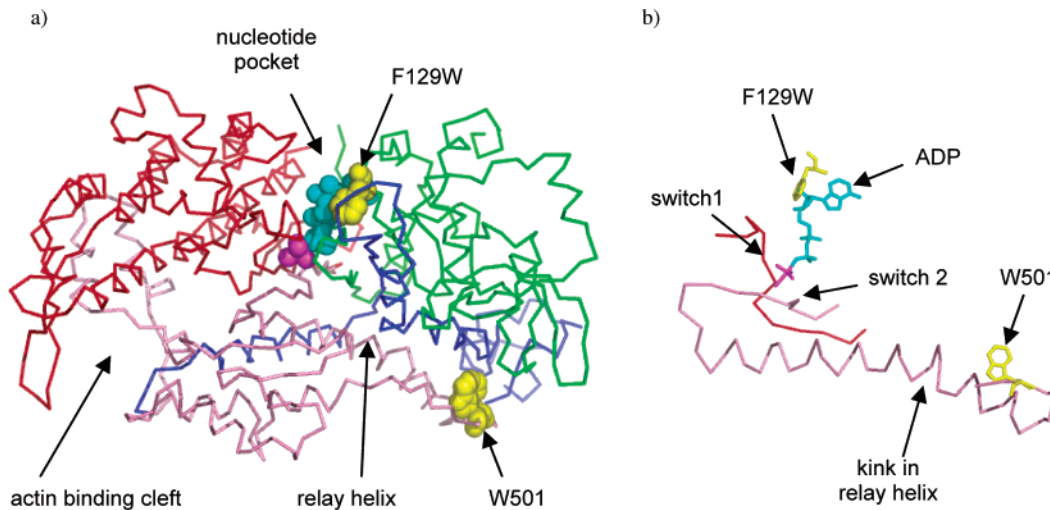
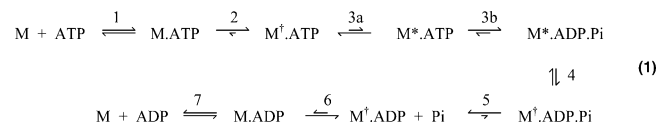


FIGURE 1: (a) The structure of the *Dd* M·ADP·Vi complex (50) to show the location of the key subdomains and tryptophan residues. Color scheme: 25K N terminal domain, green; upper 50K domain, red; lower 50K domain, pink; 20K C-terminal domain, blue. ADP, cyan; Vi, magenta. tryptophan, yellow. (b) Main chain restricted to switch 1 loop, switch 2 loop and the relay helix (in a slightly different rotation to (a)) to show the connectivity between switch 2 and W501. The switch 1 and 2 are both closed in this complex and are within bonding distance of the Vi.

yield than those that favor the closed state (6, 10, 11). During the turnover of ATP itself, the initial ATP binding step leads to a low fluorescent form, but the hydrolyzed tightly bound products complex, which represents the predominant steady-state intermediate, shows a high fluorescence. This transition gives rise to the fluorescence enhancement associated with the hydrolysis step, first noted in the 1970s (3, 12, 13), and appears to be a property of all myosins with a conserved relay-loop tryptophan. More recent kinetic analysis indicates that the fluorescence enhancement is actually associated with the step immediate prior to hydrolysis (6, 10, 14) and supports the notion that switch 2 must move first to bring the catalytic residues close enough to the  $\gamma$ -Pi to allow the chemical reaction to proceed (5, 7). In particular, non- or slowly hydrolyzable analogues, such as AMP·PNP and ATP $\gamma$ S, give intermediate fluorescence enhancements because the switch 2 closed state is partially occupied (6, 10). Temperature- and pressure-jump experiments show that the W501 side chain rapidly fluctuates between these two environments on the time scale of 1 ms, with an equilibrium constant between the open and closed states of the order of 0.5 (6, 14). To date, these two analogues have led only to crystal structures in the switch 2 open form, but it would not be surprising if crystals were produced in the closed state. Indeed, the ADP·BeF<sub>x</sub> state has been crystallized in both forms (15), supporting the finding that they are energetically similar states. In the case of ATP, the subsequent hydrolysis step pulls the equilibrium over toward the closed state, but this reaction also is reversible (16).

There is no indication that ADP induces the closed state. No relaxations transients were detected in perturbation experiments (6). Likewise apo myosin is essentially exclusively in the open state. However, in the case of *Dd* myosin II, the W501 environment is altered on ADP binding and gives rise to a rapid 10–20% quench in fluorescence of the single tryptophan construct (W501+) (10). This change reflects an earlier transition (step 2) in the scheme. These findings led to the following scheme for the *Dd* myosin ATPase, where † represents a 10–20% quench and \* a 50–

100% enhancement in W501 emission intensity (the magnitude depends on the band-pass of the detector).



The equilibrium constant  $K_{3a}$  can be assessed from the observed fluorescence signal for any nucleotide bound state, using the ADP complex as a reference for the 100% (†) open switch 2 state and the ADP·AlF<sub>4</sub> complex as a reference for the 100% (\*) closed switch 2 state (6, 11, 17). In addition, the isomerization step 2 has been monitored with a single-tryptophan construct, W129+, in which the probe is located at the entrance to the nucleotide-binding pocket. W129 revealed a large (55%) fluorescence quench on either ATP or ADP addition that allowed the resolution of step 2 into at least two processes, 2a and 2b, with forward rate constants of the order of 1000 and 350 s<sup>-1</sup>, respectively (18).

In principle, the tryptophan fluorescence can be used also to characterize the equivalent reactions in the presence of actin. There are, however, a number of practical difficulties. Actin contains four tryptophan residues per G-subunit that contribute to background fluorescence, so reducing the signal-to-noise of the measurement. Furthermore, it is possible that the actin tryptophan residues are themselves perturbed on interaction with myosin, giving rise to additional transient signals. Even if the actin tryptophans are not significantly perturbed, the association and dissociation steps are accompanied by large changes in light scatter that can give rise to artifacts in the fluorescence detection channel. A final general problem is that actomyosin-nucleotide ternary complexes are inherently unstable, leading to dissociation of the actin or the nucleotide. Conditions are required to stabilize such ternary complexes for a sufficient period to characterize their fluorescence properties. Here we address these problems and find that actin has a relatively minor influence (less than 3-fold) on the forward rate constant of the isomerization step 2 and the equilibrium constant  $K_{3a}$ .

We also report on a tryptophanless myosin construct (W-) as a control for contribution from the actin tryptophan residues and artifacts arising from light scatter.

Our findings have implications for the mechanism of actin acceleration of product release and the coupling to the return lever arm swing that constitutes the working stroke. Previous considerations led to the view that actin binding favored the switch 2 open state to facilitate phosphate release (5). We offer an alternative view in which actin has no direct influence on the position of switch 2 nor the lever arm, but coupling is achieved indirectly by activation of Pi release via switch 1 movement (i.e., switch 2 opens in response to loss of Pi). More recently, structural evidence has been advanced to suggest that actin binding and subsequent rotation of the upper 50K domain, to yield the strong binding state, decouples the switch 2 position from the lever arm orientation (8). In this scenario, the working stroke occurs concomitantly with strong actin binding and prior to phosphate release. We evaluate this model in the light of our W501 fluorescence data.

## METHODS

**Proteins.** *Dd* myosin motor domains (M761) were prepared as described previously (10, 18). The constructs used here are W- (W36F, W432F, W501F, and W584F), W501+ (W36F, W432F, and W584F) and W129+ (W36F, F129W, W432F, W501F, and W584F). Yields were typically 10 mg per preparation (30 g of cells). F-actin was prepared from rabbit skeletal muscle by the method of Spudich & Watt (19).

**Fluorescence Measurements.** Steady-state fluorescence measurements were carried out using an SLM 48000 fluorometer equipped with a 200 W Hg-Xe lamp. Stopped-flow transients were recorded on an Applied Photophysics SX18MV instrument with either a 150 W Hg-Xe lamp or a 150 W Xe lamp with excitation at 297 or 295 nm, respectively. Generally, WG335 and UG11 filters were used in the emission channel. A WG320 filter, as used in our previous studies (10, 18), was not suitable for measurements in the presence of actin. Polarized light intensities were measured using the Applied Photophysics T-adaptor with a Glans-Thomson prism in the excitation path. In this arrangement, the emission filters were placed between the polaroid filters and the detectors. Light scattering was measured at 90 degrees, either by setting the excitation monochromator to  $\geq 330$  nm or by removing the emission filter and illuminating at 297 nm. On limited occasions, light scattering was measured simultaneously with fluorescence via two independent photomultipliers housed in a custom-built holder, based on the same T-geometry as the polarization attachment. This enabled a direct comparison of the signals but, because of the 10-fold lower light throughput and reduced signal-to-noise, this method was not used routinely. For the data shown here, a 20  $\mu$ L observation cell with a 1.5 ms dead time was used to maximize the measured signal relative to the scattering background and to avoid mixing artifacts. Most transients shown are averages of 10 to 15 records. This was necessary in view of the increased background with actin present and the correspondingly smaller relative fluorescence changes. The raw signal was minimally filtered (time constant generally from 200  $\mu$ s to

1 ms and always with a time constant  $< 1/5$  of that of the fastest process to be monitored). Records were usually captured on a logarithmic timebase with oversampling, such that processes on both the millisecond and second time scales could each be fitted with similar weighting. Within individual figure panels, the high voltage on the photomultiplier was kept constant and a known offset applied, so that the signals in the presence of actin remained on scale. In the records shown, the total signal voltage is plotted after correction for the offset, so that the magnitudes of the changes in amplitude can be compared directly in the presence and absence of actin. Stated concentrations refer to the reaction chamber. Buffer conditions were 40 mM NaCl, 2 mM MgCl<sub>2</sub>, 20 mM HEPES, pH 7.5 at 20 °C, unless otherwise stated.

**Kinetic Analysis.** Data were analyzed by fitting to one or more exponential functions using Kaleidagraph (Synergy Software, Pennsylvania). Simulations and numerical fitting to kinetic schemes were carried out using Berkeley Madonna software ([www.berkeleymadonna.com](http://www.berkeleymadonna.com)).

## RESULTS

**Contribution of Actin Fluorescence to the Signal.** A comparison of the integrated fluorescence emission intensity of actin and the W501+ construct at equimolar concentrations gave a ratio of about 4:1, in line with their tryptophan contents. The W129+ construct showed about 56% the emission intensity of the W501+ construct (18). It is therefore to be expected that the equimolar actin will passively reduce the relative change in any signal from a single tryptophan in a myosin construct by 5–10-fold. The large nucleotide-induced changes in fluorescence intensity observed previously with myosin alone (10 to 100%, depending on the construct, nucleotide and filters used) should therefore still be detectable, but the relative amplitude will be reduced to within the range of 1 to 20% of the total fluorescence plus or minus any actin-mediated changes in the tryptophan fluorescence.

**Controls with the W- Construct.** To interpret any fluorescence changes observed with W129 and W501, it is necessary to assess the relative contribution from sources other than the tryptophan residues within the myosin heads. Previous studies showed that the W- construct has a fluorescence emission spectrum characteristic of tyrosine and that for excitation at  $\geq 295$  nm, the emission intensity at 340 nm was negligible ( $\leq 10\%$ ) compared with that from W501 and W129 (10). This construct therefore provides a suitable control.

On mixing actin with equimolar W- in the stopped-flow apparatus, an apparent fluorescence enhancement was observed whose amplitude was 3–4% of the signal (Figure 2a). The enhancement appeared in phase with the accompanying increase in light scattering attributed to protein association and had an apparent second order rate constant of approximately 1  $\mu$ M<sup>-1</sup> s<sup>-1</sup>. Addition of 1 mM ATP to the preformed actoW- gave a quantitative reversal of the apparent enhancement as expected for complete dissociation of the protein complex. The quenching process, also, appeared in phase with the corresponding light scattering transient (Figure 2b).

The apparent fluorescence changes could reflect changes in actin tryptophan fluorescence and/or a light scattering

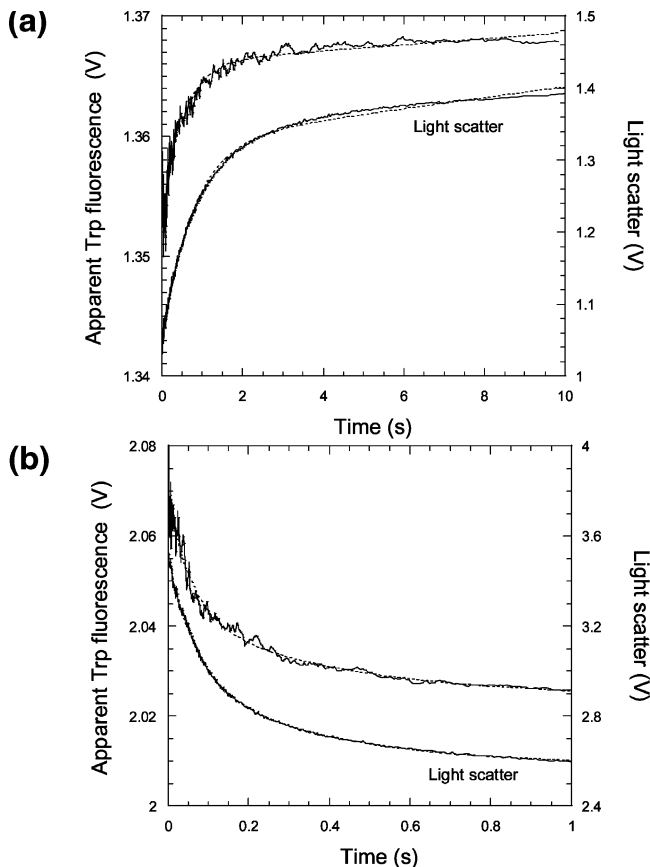


FIGURE 2: Stopped flow transients on interaction of tryptophanless myosin construct (W-) with F-actin. (a) The apparent tryptophan fluorescence transient (upper trace) and light scattering transient (lower trace) acquired on mixing  $3 \mu\text{M}$  W- construct with  $2 \mu\text{M}$  actin, each fitted to a single exponential with a sloping end-point to yield rate constants of  $2.0$  and  $1.3 \text{ s}^{-1}$ , respectively. The data were also well fit by a hyperbola as might be expected because the reactants in the second-order reaction had similar concentrations. (b) The apparent tryptophan fluorescence transient (upper trace) and light scattering transient (lower trace) acquired on mixing  $1 \mu\text{M}$  acto-W- with  $50 \mu\text{M}$  ATP, fitted to double exponentials to yield rate constants of  $16 \text{ s}^{-1}$  plus  $2.4 \text{ s}^{-1}$  (fluorescence) and  $15 \text{ s}^{-1}$  plus  $3 \text{ s}^{-1}$  (light scatter). The experiment was conducted at  $297 \text{ nm}$  Hg-Xe excitation. Control experiments with scattering solutions suggest that the observed signal in the tryptophan channel has a significant contribution from emission filter fluorescence induced by scattered light (see text).

artifact. The scattered light signal from actoW- is about 10 times more intense than the fluorescence signal and decreases by a factor of 2 on actoW- dissociation. Therefore, a breakthrough of just 1% stray light from scattering would be sufficient to give a 5% change in the total signal in the fluorescence channel, and this would dominate the profiles recorded in Figure 2. There are three potential light scatter artifacts that might contribute to a signal in the fluorescence channel. (1) The  $297 \text{ nm}$  excitation light may contain stray light at wavelengths  $>335 \text{ nm}$ , which is transmitted by the emission filter. (2) The emission filter may transmit a small but significant amount (around 1%) of  $297 \text{ nm}$  light. (3) The scattered  $297 \text{ nm}$  light may induce fluorescence or phosphorescence in the emission filter (20), which is then detected by the photomultiplier. The first source was ruled out by including a  $297 \text{ nm}$  narrow band-pass interference filter (297FS10-25 Andover Corporation, LOT Oriel Ltd.) in series with the excitation monochromator. Although the overall

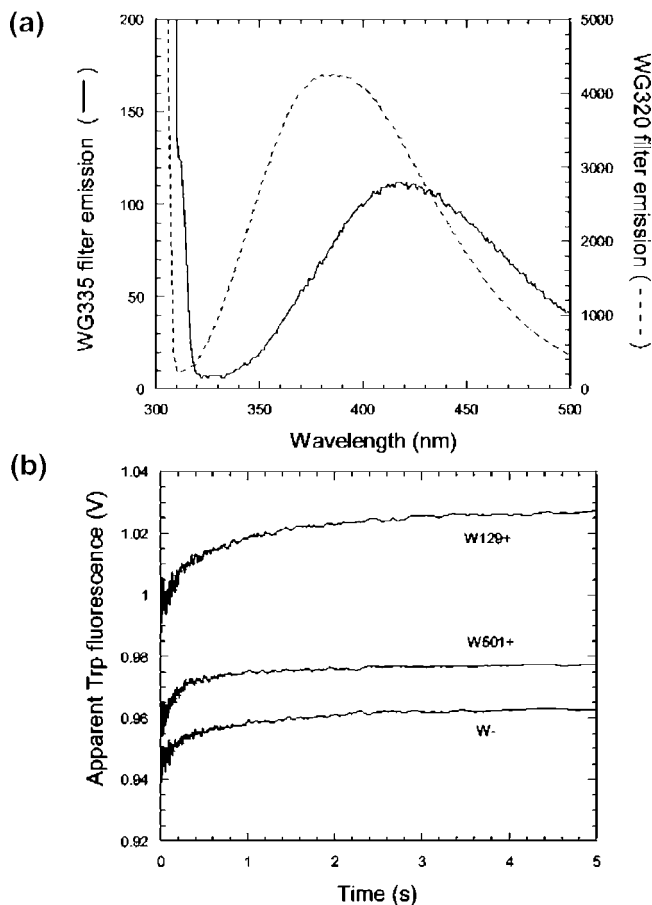


FIGURE 3: (a) Fluorescence emission spectra for WG335 and WG320 cutoff filters. The filters were excited at  $297 \text{ nm}$  and positioned to minimize direct reflection of the excitation light toward the detector channel. Note the different scales for the two filters. (b) Fluorescence transients observed upon mixing  $2 \mu\text{M}$  actin with  $3 \mu\text{M}$  W- (lower trace),  $5 \mu\text{M}$  W501+ (middle trace) and  $3 \mu\text{M}$  W129+ (upper trace). The absolute amplitudes of the observed transients,  $0.016 \text{ V}$  (W-),  $0.017 \text{ V}$  (W501), and  $0.025 \text{ V}$  (W129) can be compared directly because the instrument parameters were the same. Control experiments with scattering solutions suggest that the observed signals have a significant contribution from emission filter fluorescence induced by scattered light. The experiment provides an upper limit on the extent to which W501 and W129 fluorescence is specifically perturbed by actin on forming the rigor complex. ( $<5\%$  with respect to a single myosin tryptophan residue).

emission signal was reduced, the relative change in the fluorescence channel was unaffected compared with the records in Figure 2. The second source was ruled out by independent measurement of the transmission of the WG335 nm cutoff filter in a Cary 50 spectrophotometer. This measurement showed the transmittance at  $297 \text{ nm}$  was  $\leq 0.005\%$ , close to the detection limit of the instrument. This would be sufficient to block  $297 \text{ nm}$  light itself. However, the transmission reading increased as the filter was moved closer to the detector. This suggests there was significant light emission from the filter. When excited at  $297 \text{ nm}$  in a fluorescence spectrophotometer, emission from the WG335 filter was detected across the near UV-visible region, peaking at  $415 \text{ nm}$  (Figure 3a). Emission from a WG320 filter was 40 times more intense and peaked at  $385 \text{ nm}$ . This filter was therefore avoided. In the case of the stopped-flow apparatus, the photomultiplier faceplate is within  $5 \text{ mm}$  of the emission filter to maximize photon capture and hence this apparatus

is very susceptible to filter fluorescence. Substitution of a 365 nm band-pass interference filter (Omega 365HT25, Glen Spectra Ltd) in front of the emission detector did not improve the situation significantly, and the tests described above indicated that this filter also suffered from fluorescence emission.

With a glycogen scattering solution in the stopped flow apparatus, at a concentration that matched the scattering from a 2  $\mu\text{M}$  actoW- solution, the stray light detected in the fluorescence channel through the band-pass filter was comparable to the changes in signal detected in Figure 2. The use of cross polarizers to block the scattered 297 nm light from reaching the emission filter was also examined, and appeared to reduce the artifact, but the overall transmission of the true fluorescence signal was so low that the changes of the magnitude in observed in Figure 2 could not be reliably detected. Overall, we conclude that a scatter artifact arising from far-UV-induced fluorescence in the emission filter could account for the signals observed in the tryptophan channel of Figure 2 and, therefore, that there is no reason to invoke any change in actin tryptophan fluorescence on binding the W- construct. Nevertheless, this signal is important to characterize, as it will occur in all experiments involving actomyosin samples described below and will be coincident with the protein association or dissociation phase of the reaction.

On mixing either W129+ or W501+ constructs with actin, similar transients were observed (Figure 3b) to those seen with W- (Figure 2a). The amplitudes of the signals were marginally larger for the W129+ construct (by 1.5-fold) and the W501+ construct (by 1.1-fold) than for W-, which could indicate that the myosin tryptophans were perturbed. However, variations in the scattering signal with different preparations are a more likely cause.

*The Effect of Actin on Step 2 ( $M^i$  Formation). ATP Binding.* Figure 4 compares the effect of mixing the W129+ construct with 1 mM ATP in the presence and absence of equimolar actin. In the absence of actin, a quench in tryptophan fluorescence occurred with an observed rate constant of 295  $\text{s}^{-1}$  and amplitude of 0.1 v. This corresponds to the slower of the two subcomponents observed previously (18), because with the larger cell used here most of the faster subcomponent of 1800  $\text{s}^{-1}$  is lost in the dead-time. The latter would be expected to have an amplitude of around 0.2 v, based on previous measurements (18). When 1 mM ATP was mixed with acto-W129+, the observed fluorescence quench had a larger amplitude (0.3 v) and slower rate constant (86  $\text{s}^{-1}$ ). The latter was similar to the rate constant for the light scattering signal (100  $\text{s}^{-1}$ ) that monitors the dissociation reaction. The observed rate constants were near saturated with respect to [ATP] under these conditions. It appears that the process involved in step 2 (or at least step 2b) is slowed so that it now controls the rate of dissociation of the ternary acto-W129+•ATP complex. However the tryptophan fluorescence signal observed in the presence of actin has a significant contribution (2–4% of the total fluorescence) from the dissociation process itself (as characterized in the experiments with W- above). Comparison of the observed (0.3 v) and expected total (0.2 v {2a} + 0.1 v {2b} +  $\leq$  0.1 v {dissociation}) amplitude suggests that step 2b is slowed 3-fold in the presence of actin, while the fast phase may also contribute (cf. in the absence of actin

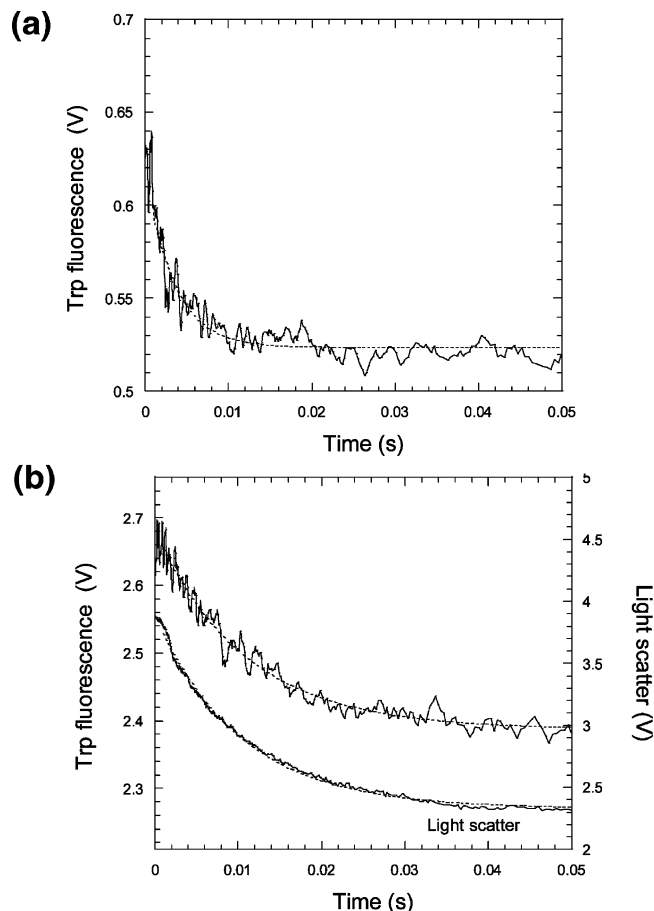


FIGURE 4: Stopped-flow transients on mixing W129+ with ATP in the absence and presence of actin. Single-exponential fits are shown superimposed. (a) 2  $\mu\text{M}$  W129+ was mixed with 1 mM ATP to yield  $k_{\text{obs}} = 295 \text{ s}^{-1}$  (amplitude = 0.1 V). (b) 2  $\mu\text{M}$  acto129 was mixed with 1 mM ATP. Fluorescence (upper trace) yielded  $k_{\text{obs}} = 91 \text{ s}^{-1}$  (amplitude = 0.29 V) and light scattering (lower trace),  $k_{\text{obs}} = 97 \text{ s}^{-1}$ . Excitation was at 295 nm with a Xe lamp. Absolute amplitudes of tryptophan signals are directly comparable in (a) and (b).

where 2a is largely lost in the dead-time). Nevertheless, the variability of the scattering signal amplitude and its effect on the fluorescence signal precludes an unambiguous conclusion. Fortunately, more definitive information about the effect of actin on step 2a and 2b can be obtained with other nucleotides, as described below.

*ADP Binding.* Figure 5 compares the effect of mixing the W129+ construct with ADP in the presence and absence of equimolar actin. In the absence of actin, the processes observed are similar to those seen with ATP, as noted previously (18). ADP induces only limited actin dissociation (<10% dissociation, as judged by the relatively small amplitude of light scattering transient), and this occurs on a much slower time scale ( $k_{\text{obs}} < 0.1 \text{ s}^{-1}$  cf. 100  $\text{s}^{-1}$  for ATP). Consequently, the more rapid processes induced by nucleotide binding per se can be readily resolved. In this case, it is clear that actin had no significant effect on the amplitude of the W129 signal and the observed rate constant was slowed by less than 2-fold. A 10-fold lower nucleotide concentration was used in this case (100  $\mu\text{M}$  ADP cf. 1 mM ATP in Figure 4) to minimize the contribution from contaminating ATP. However, similar findings were observed at 1 mM ADP, with only marginal (2-fold) increases in the observed rate constants. The data clearly demonstrate

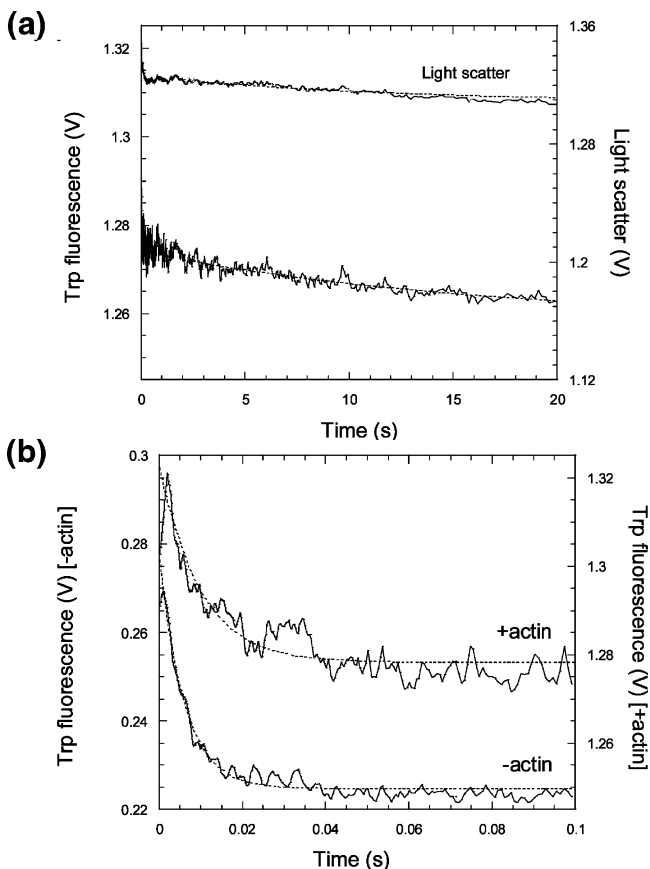


FIGURE 5: Transients observed on mixing  $1 \mu\text{M}$  W129+ or acto-W129+ with  $100 \mu\text{M}$  ADP. The latter was pretreated with hexokinase and glucose to remove contaminating ATP (2 mM glucose plus  $2 \mu\text{g}$  hexokinase per 5 mL of  $200 \mu\text{M}$  ADP for 5 min). (a) Comparison the light scattering (upper trace) and fluorescence (lower trace) transients for acto-W129+ on the time scale of actin dissociation. Single-exponential fits for data points  $> 2$  s are shown superimposed, with  $k_{\text{obs}}$  values of  $0.06 \text{ s}^{-1}$  (fluorescence) and  $0.09 \text{ s}^{-1}$  (light scatter), although these are not well defined because of the small amplitudes. (b) Comparison of W129+ and acto-W129+ on mixing with ADP on a faster time scale. The Y-axes are displaced owing to the extra fluorescence signal from actin but the scales are directly comparable. Single-exponential fits are shown superimposed, with  $k_{\text{obs}}$  values of  $168 \text{ s}^{-1}$  (lower trace - actin) and  $103 \text{ s}^{-1}$  (upper trace + actin) and fitted amplitudes of  $0.053 \text{ V}$  (- actin) and  $0.045 \text{ V}$  (+ actin). Excitation was via 297 nm Hg-Xe lamp with emission monitored via the dual wavelength attachment.

that step 2 equivalent, as sensed by W129, does not become rate-limiting for dissociation.

**ATP $\gamma$ S Binding.** Figure 6 shows the corresponding experiment with ATP $\gamma$ S. In the absence of actin, the observed tryptophan fluorescence quench appeared similar to that observed with ATP, but the rate constants for the steps equivalent to 2a and 2b were slowed by about 2–3-fold. Consequently, less of the fast phase was lost within the dead-time of the stopped-flow apparatus. Nucleotide-induced actomyosin dissociation is similar in its extent to that observed with ATP, but occurs on a 50–100-fold slower time scale, intermediate between that observed for ATP and that for ADP. Thus, the more rapid processes induced by nucleotide-binding per se can be resolved from dissociation. The data shown here at  $100 \mu\text{M}$  ATP $\gamma$ S revealed two subcomponents in approximately equal proportions with  $k_{\text{obs}}$  values of around 700 and  $105 \text{ s}^{-1}$ , together with a slow phase

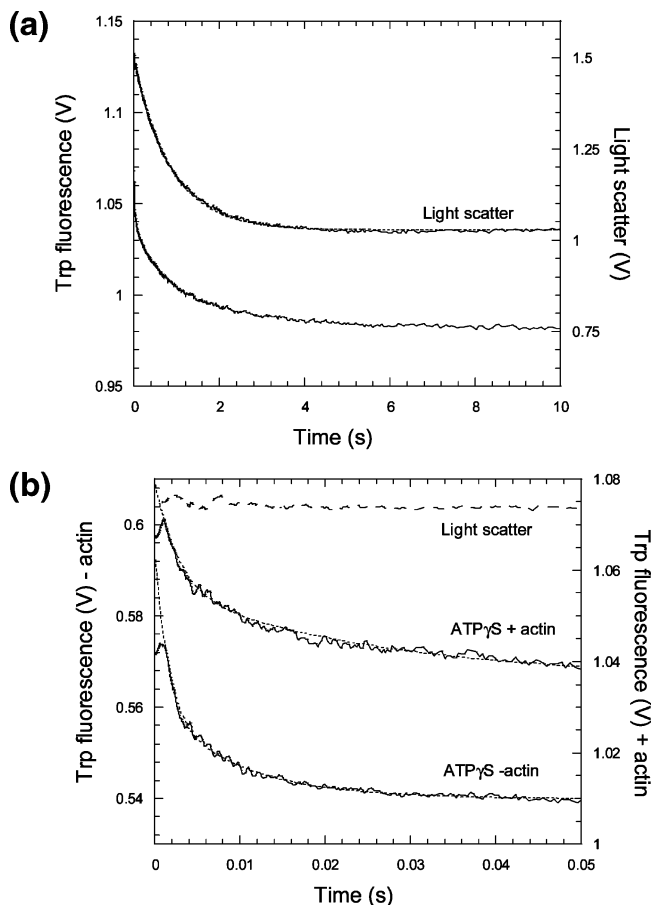


FIGURE 6: Transients observed on mixing  $1 \mu\text{M}$  W129+ or acto-W129+ with  $100 \mu\text{M}$  ATP $\gamma$ S. (a) Comparison of the light scattering (upper trace) and fluorescence (lower trace) transients for acto-W129+ on the time scale of actin dissociation. Single-exponential fits yielded rate constants of  $1.2 \text{ s}^{-1}$  (light scattering) and  $0.7 \text{ s}^{-1}$  (fluorescence). (b) Comparison of tryptophan fluorescence on mixing W129+ (lower trace) and acto-W129+ (middle trace) with  $100 \mu\text{M}$  ATP $\gamma$ S on a faster time scale. The Y-axes are displaced owing to the extra signal from actin but the scales are directly comparable within this panel. Double exponential fits are shown superimposed, with  $k_{\text{obs}}$  values of  $723 \text{ s}^{-1}$  (amplitude  $0.035 \text{ V}$ ) and  $104 \text{ s}^{-1}$  (amplitude  $0.020 \text{ V}$ ) (- actin), and  $377 \text{ s}^{-1}$  (amplitude  $0.024 \text{ V}$ ) and  $39 \text{ s}^{-1}$  (amplitude  $0.020 \text{ V}$ ) (+ actin). The dashed line shows there was no light scattering change on this time scale (plotted on same scale as light scatter in panel (a)). Excitation was via 297 nm Hg-Xe lamp. The UG11 was omitted in this case, thus explaining the small relative signal changes compared to other experiments.

( $0.8 \text{ s}^{-1}$ ) with a small amplitude (22% of the total). In the presence of actin, the corresponding rate constants were 380 and  $39 \text{ s}^{-1}$ , but now the slowest phase ( $0.76 \text{ s}^{-1}$ ) had a 6-fold larger amplitude and was near coincident with the dissociation reaction ( $1 \text{ s}^{-1}$ ). The increase in amplitude of the slowest phase in fluorescence is accounted for by the contribution from the dissociation reaction itself (i.e., the light scatter artifact). The biphasic fast process appear to be directly related to that observed in our previous studies with ATP and ADP in the absence of actin (18), because the amplitude ratio of the two subcomponents titrated with [ATP $\gamma$ S] in a qualitatively similar manner and no additional faster process became apparent when the  $5 \mu\text{L}$  cell (with a 0.5 ms dead time) was used. Our previous data were modeled with a two-step expansion of step 2, together with an additional off-line binding step (18). The latter gave rise to a small rapid

transient at all nucleotide concentrations, but this would be lost in the longer dead-time cell used in the presence of actin.

These data lead to an overall similar conclusion to those deduced from experiments with ATP and ADP. Namely, actin has a minor effect on step 2a and step 2b, and the latter is slowed by no more than 3-fold and the process sensed by W129 does not limit the rate of dissociation of actin by ATP $\gamma$ S.

**Nucleotide Binding to the acto-W501+ Construct.** In the absence of actin, ATP binding to the W501+ construct results in a large (50–100%) fluorescence enhancement. Essentially, this process monitors the effective hydrolysis step (i.e., overall step 3 in Scheme 1). The more rapid formation of M<sup>†</sup>•ATP is accompanied by 10% quench, but this is offset by an enhancement owing to formation of a limited amount of M\*•ATP ( $K_{3a} \sim 0.3$ ). The rate of formation of both states is controlled by  $k_{+2}$  at around 350 s<sup>-1</sup>, with M<sup>†</sup>•ATP and M\*•ATP remaining in rapid equilibrium. Overall, this initial process is almost optically silent at 20 °C because the signal from M\*•ATP formation practically balances that from M<sup>†</sup>•ATP (10, 17). In practice, a brief lag phase or a small burst in the enhancement phase may be observed depending on the exact conditions and preparation. The amplitude of this phase is, however, small compared with the subsequent slower enhancement associated with the hydrolysis phase. At low temperatures,  $K_{3a}$  is reduced to <0.1, allowing the transient formation of M<sup>†</sup>•ATP to be partially resolved as a small quench in fluorescence before the slower rise due to limited hydrolysis (6, 10).

**ATP Binding.** Figure 7 shows the results of mixing ATP with the W501+ construct at 20 °C. In the presence of actin, the light scatter signal indicates that dissociation occurs more rapidly than the W501 enhancement (Figure 7a), although the processes are not well resolved. The light scatter signal also has a slow phase, possibly related to dissociation of bundled filaments (21, 22). Note that the expected light scatter artifact is now operating in the opposite direction to the W501 enhancement and thus will reduce the observed fluorescence amplitude, particularly in the early phase. The tryptophan signals on mixing the W501+ construct with ATP in the absence and presence of actin are compared in Figure 7b, which, when fitted to a single exponential, yielded  $k_{obs}$  values of 36 and 19 s<sup>-1</sup>, respectively. However, in the absence of actin the profile fitted better to a double exponential to yield rate constants of 235 and 20 s<sup>-1</sup> (with an amplitude ratio of 1:1.5). On the other hand, with actin present, the total amplitude was reduced and only a single process was observed similar to the slower of the two phases observed in its absence. The lack of effect on the observed rate constant of the latter is consistent with actin dissociation preceding hydrolysis, as in the classical Lymn-Taylor scheme (23). The observed effects on the fast phase can be reconciled with the light scatter artifact that occurs on actin dissociation nullifying the enhancement arising from limited M\*•ATP formation. As a more direct test of this explanation, the experiment was carried out at 2 °C where, in the absence of actin, an initial fluorescence quench is observed (Figure 7c) owing to the M\*•ATP state being much less occupied compared with M<sup>†</sup>•ATP. In the presence of actin, the initial quench does become more prominent and provides a more direct indication of a second quenching process with an

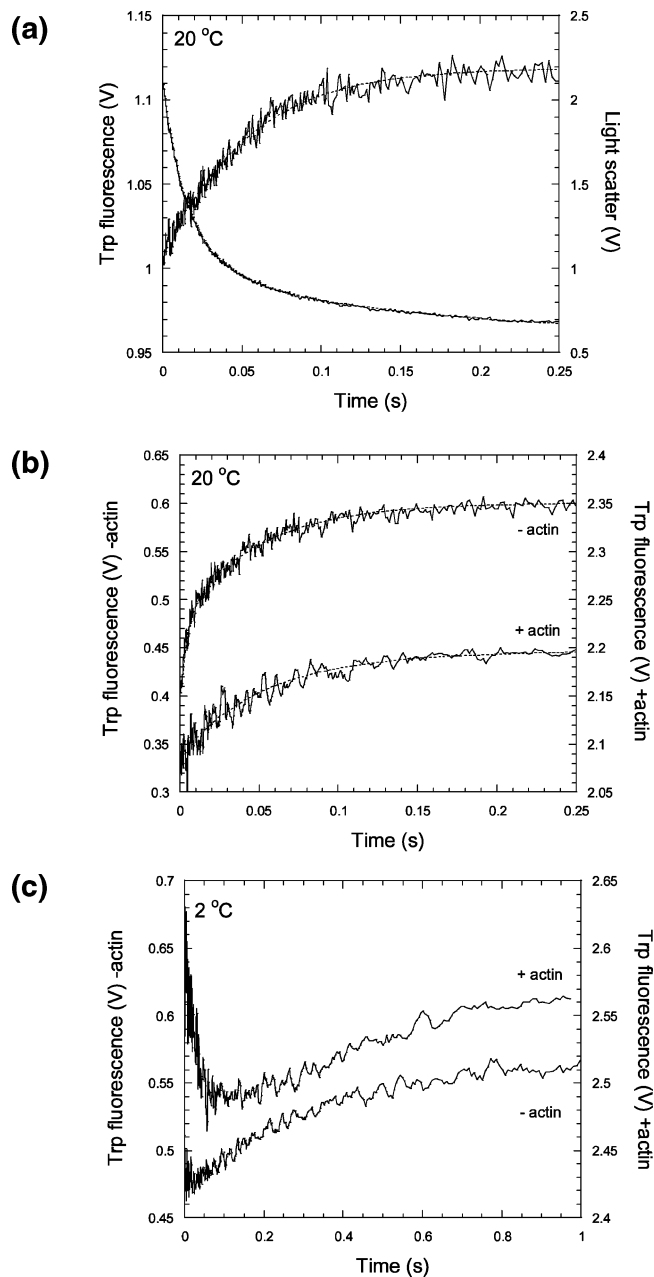


FIGURE 7: Transients observed on mixing 1  $\mu$ M W501+ or acto-W501+ with 1 mM ATP at (a, b) 20 °C or (c) 2 °C. (a) Comparison of the tryptophan fluorescence signal and light scatter when acto-W501+ was mixed with 1 mM ATP. The light scatter transient was fit with a biexponential with rate constants 56 s<sup>-1</sup> (amplitude 0.98 V) and 6.6 s<sup>-1</sup> (amplitude 0.42 V) while the fluorescence trace was fit to a single exponential with rate constant 18 s<sup>-1</sup>. (b) Comparison of the tryptophan fluorescence transients in the presence and absence of actin. This was a different preparation to that used in (a). The transients were fitted to a double exponential in the absence of actin (lower trace) to yield rate constants of 235 s<sup>-1</sup> (amplitude = 0.08 V) and 20 s<sup>-1</sup> (amplitude 0.12 V) and to a single exponential in the presence of actin (upper trace) to yield a rate constant of 19 s<sup>-1</sup> (amplitude 0.11 V). (c) Same experiment as (b) and with the same instrument settings but conducted at 2 °C. Note the small quench at the start of the reaction in the absence of actin, as noted previously (10) becomes much more pronounced in the presence of actin owing to a contribution of the signal from the actin dissociation reaction and/or shift in myosin conformation to the open state.

additive contribution. Given the relatively large subsequent enhancement phase, the underlying quenching process(es) cannot be precisely quantified, but the observed effects are

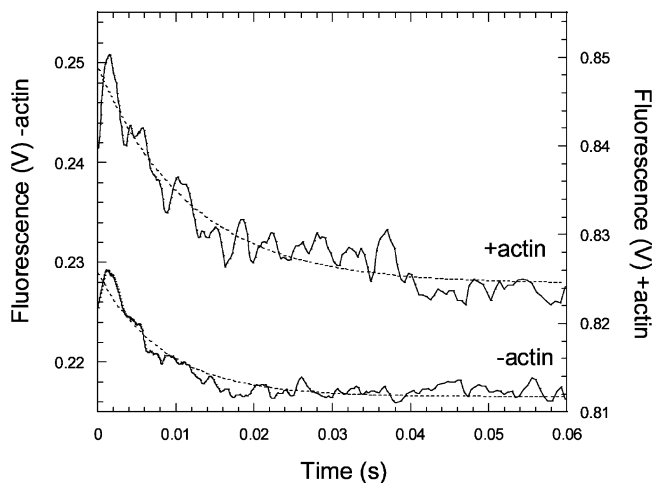


FIGURE 8: Transients observed on mixing  $1 \mu\text{M}$  W501+ or acto-501+ with  $100 \mu\text{M}$  ADP. The latter was pretreated with hexokinase as in Figure 5. The Y-axes are displaced owing to the extra signal from actin but the scales are directly comparable. Single-exponential fits are shown superimposed, with  $k_{\text{obs}}$  values of  $189 \text{ s}^{-1}$  (– actin) and  $90 \text{ s}^{-1}$  (+ actin) and fitted amplitudes of  $0.0165 \text{ V}$  (– actin) and  $0.0247 \text{ V}$  (+ actin). Only data points beyond 2 ms are fitted. Light scattering is not shown but was similar to that in the corresponding W129+ experiment (Figure 5) as was the instrumentation used.

in line with the expected magnitude of the contribution from actin dissociation alluded to above.

**ADP Binding.** Figure 8 shows the corresponding experiment with the W501+ construct and ADP. In the absence of actin, a 10% quench is observed with kinetics similar to the process observed from W129. Previous studies have shown that there is no significant occupancy of the closed state under these conditions i.e., step 3a is highly unfavorable, and hence the observed quench has been attributed to step 2 (6, 10). The data presented here demonstrate a similar process occurs in the presence of actin. The quench is 1.5-fold larger with actin present and the rate constant reduced by 2, but this is within experimental variability. The lack of any major effect is perhaps not surprising given that none was observed with W129, which is assumed to be monitoring the same step. However, these data do indicate that W501 responds to step 2 in a qualitatively similar manner when actin is bound and that the closed state remains unoccupied. Nucleotide-induced dissociation does not contribute to the transients shown here because it occurs on a much slower time scale, as with the acto-W129+ construct.

**ATP $\gamma$ S Binding.** Previous studies with ATP $\gamma$ S showed neither a significant quench nor enhancement of W501 fluorescence at  $20^\circ\text{C}$  and suggested that the major steady-state species existed in equilibrium between open and closed states with  $K_{3a}$  of the order of 0.3 in the absence of actin (10, 11). This analogue therefore offers a good opportunity to measure the effect of actin on the open-to-closed equilibrium, particularly as the data with the W129+ show that the dissociation reaction is 2 orders of magnitude slower than the binding isomerizations. No major effect on this equilibrium was apparent with ATP (Figure 6), but this may reflect the relatively rapid dissociation of actin, such that the open-to-closed transition could reequilibrate according to its position in the absence of actin. Consequently, no rigorous conclusion can be drawn as to the effect of actin on the  $K_{3a}$  other than that A.M\*•ATP does not become a dominant

intermediate. The relatively slow actin dissociation with ATP $\gamma$ S presents a convenient approach to address this ambiguity.

Figure 9a shows the scaled fluorescence transients induced on mixing the W501+ construct with ATP and ATP $\gamma$ S. At  $20^\circ\text{C}$ , ATP $\gamma$ S yields only a small enhancement compared with that of ATP, in line with earlier studies (10). Comparison of the ATP $\gamma$ S record with simulated data (17) indicates that  $K_{3a}$  is between 0.2 and 0.3 and that the hydrolysis reaction (step 3b) is slow and reversible such that it does not “pull” the step 3a equilibrium over toward the enhanced M\*•ADP•Pi state to any great extent. In the presence of actin, the fluorescence transient shows an overall small reduction in intensity on this time scale. At  $2^\circ\text{C}$ , ATP $\gamma$ S shows a clear quench in W501 fluorescence, the magnitude of which is similar to that observed with ADP (10), which indicates that the 3a equilibrium lies strongly toward the open state ( $K_{3a} < 0.05$ ). A similar profile was observed in the presence of actin at  $2^\circ\text{C}$ . The latter is an important result as it supports the conclusion that at  $20^\circ\text{C}$ , where an intermediate fluorescence signal is observed, the  $K_{3a}$  equilibrium is poised between the two extremes both in the presence and absence of actin.

The effect of actin can be quantified by assuming that the ATP induces a predominantly (80%) closed state, while ATP $\gamma$ S at  $2^\circ\text{C}$  is in a near fully open state. Comparison with simulated data suggest that actin has approximately a 2-fold effect on the equilibrium constant of step 3a at  $20^\circ\text{C}$  (17). However, it is important to determine that this conclusion is not significantly affected by the values assigned to other rate constants in the scheme. This was done by numerical fitting of the fluorescence profiles to the mechanism shown in eq 2, but with an expanded step 2. The relatively slow initial quench in fluorescence could be modeled if W501 fluorescence was sensitive to step 2b only, leaving step 2a fast but undefined. Figure 9b shows the same records for ATP $\gamma$ S at  $20^\circ\text{C}$  as in the middle traces of Figure 9a but on an expanded and absolute voltage scale. To constrain the fitting to the W501+ data, the values for steps 2a and 2b were initially set according to those reported by the W129+ construct, but allowing them to float did not alter the overall conclusion. Floating  $k_{2b}$  for the fit in the presence of actin yielded  $30 \text{ s}^{-1}$ .  $k_{2a}$  was not uniquely defined as the transition was optically silent with respect to W501, but its value was  $\gg k_{2b}$  in all solutions. The rate constant  $k_{-3a}$  was fixed at  $1000 \text{ s}^{-1}$  to ensure that step 3a remained in equilibrium relative to step 2b.  $k_{3a}$  was floated and the fitted value used to define  $K_{3a}$  ( $= k_{3a}/1000$ ). The hydrolysis steps  $k_{3b}$  and  $k_{-3b}$  were also floated, while the subsequent product isomerization step was initially set at  $0.5 \text{ s}^{-1}$  (although over the time scale shown in Figure 9b it does not contribute significantly). In the absence of actin, fitting yielded a value of  $K_{3a} = 0.26$  and values of  $k_{3b} = 4 \text{ s}^{-1}$  and  $k_{-3b} = 5 \text{ s}^{-1}$ . The latter rate constants account for the slight rise in fluorescence over the time scale of Figure 9b, with  $k_{\text{obs}} = 9 \text{ s}^{-1}$ , and suggest that hydrolysis of ATP $\gamma$ S is not a rate-limiting step per se ( $k_{\text{cat}} = 0.05 \text{ s}^{-1}$ ) (10). In the presence of actin, the fit required a decrease in  $K_{3a}$  to 0.15 and an apparent increase in  $k_{3b}$  to  $12 \text{ s}^{-1}$  and  $k_{-3b}$  to  $15 \text{ s}^{-1}$ . However, the latter is probably due to the influence of the subsequent dissociation reaction (Figure 9c), which reverses the direction of the profile and hence results in an apparent

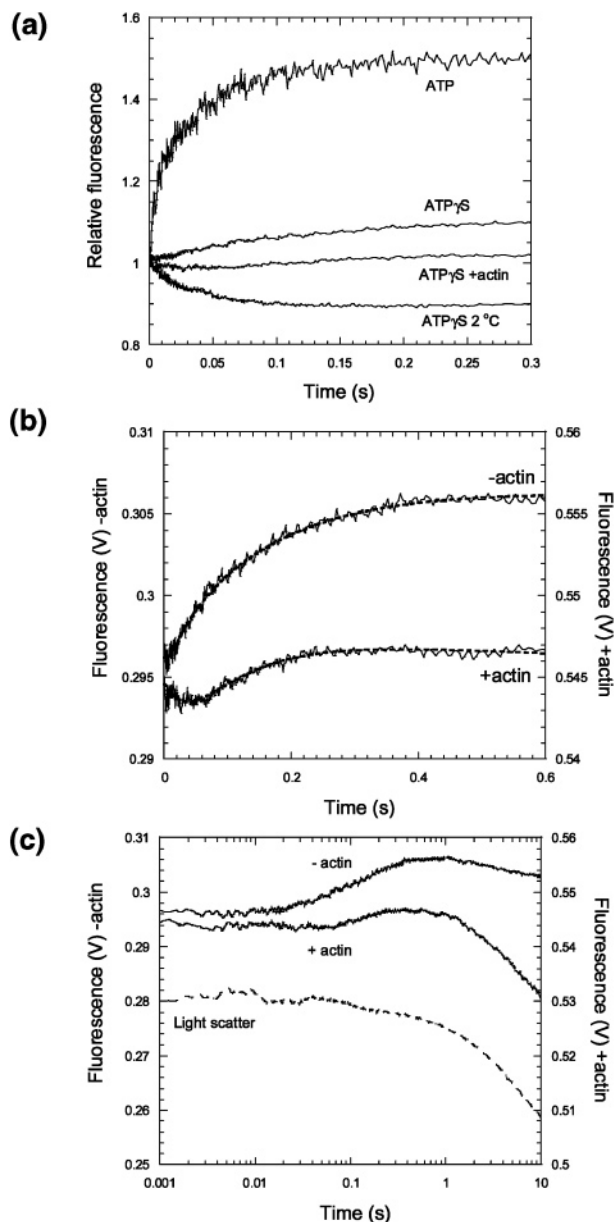


FIGURE 9: Transients observed on mixing 1  $\mu\text{M}$  W501+ or acto-W501+ with 100  $\mu\text{M}$  ATP $\gamma$ S. (a) A comparison of the fluorescence profile on mixing the 1  $\mu\text{M}$  W501+ construct with 1 mM ATP (top trace) and 100  $\mu\text{M}$  ATP $\gamma$ S (other traces). The data were normalized to show the fluorescence change relative to the apo myosin state and illustrate the relatively small enhancement induced by ATP $\gamma$ S at 20  $^{\circ}\text{C}$  in the absence of actin ( $k_{\text{obs}} = 9 \text{ s}^{-1}$ ). Addition of actin caused a small decrease in amplitude of the signal change on this time scale with a notable lag or slight initial quench (note the fluorescence contribution from actin was subtracted before normalization). At 2  $^{\circ}\text{C}$  in the absence of actin, ATP $\gamma$ S induced a net quench in fluorescence (bottom trace;  $k_{\text{obs}} = 36 \text{ s}^{-1}$ ) very similar to that observed with ADP (cf. 10) and is indicative of a largely open state (i.e.,  $K_{3a} < 0.05$ ). Increasing the ATP $\gamma$ S to 1 mM had a minor effect on the overall profiles. (b) ATP $\gamma$ S binding to W501+ in the absence and presence of actin. These are the same records as the middle traces in (a) but presented on an amplified and absolute voltage scale. The dashed lines are the numerically fitted profiles for the scheme shown in eq 2 to yield  $K_{3a} = 0.26$  in the absence of actin and 0.15 in its presence (see text for details). (c) The same records on a logarithmic time scale to show the dissociation phase ( $1.5 \text{ s}^{-1}$ ). The dashed line was the recorded light scatter signal, normalized to match the change in tryptophan fluorescence and demonstrates that very little (<5%) actin dissociation occurred on the time scale of the transients shown in (a) and (b). The instrumentation was the same as in Figure 6.

increase in the rate constant of the enhancement phase. Note that the light scatter trace in Figure 9c shows that actin remains largely bound over the early phase of the reaction used to define  $K_{3a}$  ( $< 0.1 \text{ s}$ ), but because of its influence on the fluorescence profile, it does affect the presumed hydrolysis phase (0.1–1 s) even though the half time of the dissociation reaction is an order of magnitude longer still. The reactions were therefore fitted over the entire 10 s time course with an additional fluorescence change included to model that arising from the dissociation reaction (which fitted to a rate constant of  $1.5 \text{ s}^{-1}$ ). As a result of this correction, the values for  $k_{3b}$  and  $k_{-3b}$  in the presence of actin became 3 and 4  $\text{s}^{-1}$ , respectively, similar to their values in the absence of actin, while  $K_{3a}$  remained unchanged at 0.15. Although the best-fit rate constants depended on the precise values assigned to the fluorescence of each species and uncertainties in the initial offset of the records, by exploring a range of conditions, it was clear that the change in profiles observed in Figure 9b in the presence of actin could be fit by a 1.5–2-fold change in the value of  $K_{3a}$  and that this was a robust and necessary feature of the modeling.

In the above analysis, we assumed that the rising phase in fluorescence in Figure 9b corresponds to hydrolysis ( $k_{\text{obs}} = 8 \text{ s}^{-1}$ ) and therefore this step is not rate-limiting for the overall turnover of ATP $\gamma$ S ( $k_{\text{cat}} = 0.05 \text{ s}^{-1}$ ) (10). The unfavorable equilibria of the  $K_{3a}$  and  $K_{3b}$  steps result in a limited thiophosphate burst (0.15 mol/mol M) that would be difficult to detect. The possibility of a rapid but unfavorable hydrolysis equilibrium was raised in the first study that characterized ATP $\gamma$ S kinetics with skeletal muscle myosin (12). However, subsequent oxygen exchange studies found no evidence for rapid reversal of ATP $\gamma$ S hydrolysis (24), although this could be due to restricted rotation of the thiophosphate group. If hydrolysis were slower than the observed  $8 \text{ s}^{-1}$ , it would not alter the conclusions concerning  $K_{3a}$ , but would require an additional isomerization after the open-to-closed transition. Indeed, an alternative interpretation of our data is that in the presence of ATP $\gamma$ S the open-to-closed transition is slowed by 2 orders of magnitude compared with other nucleotides and that the rising phase in fluorescence in Figure 9b reflects this process rather than hydrolysis. However, the conclusion that the value of  $K_{3a}$  is reduced by less than 2-fold by actin still holds based on the relative fluorescence level after 60 ms.

## DISCUSSION

In this work, we have characterized the influence of actin on the nucleotide-induced conformational transitions with *Dd* myosin II motor domain. The control experiments with the *Dd* tryptophanless construct, W-, demonstrate that the actin tryptophans are not greatly perturbed by myosin binding, but nonetheless, a significant signal is observed owing to a light scatter artifact. This problem appears to be caused by fluorescence induced in the emission filter and thus specifically affects instruments, such as the stopped-flow apparatus, where the photomultiplier is in close proximity to the filter. Polarization optics may help to reduce this problem, but multiple scattering within the cell reduces the effectiveness of this approach. In addition, the reduction in overall signal by the polarizers makes it difficult to characterize the low amplitude transients under investigation here. The problem of the high background fluorescence from actin

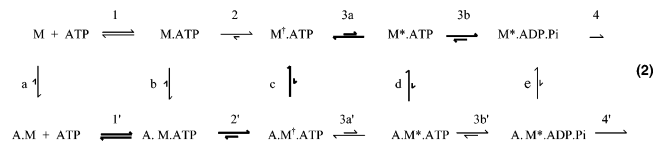
tryptophans may be circumvented by the use of actin constructs with reduced tryptophan content. Doyle et al. (25) explored the use of a tryptophanless actin construct, but this failed to polymerize normally. They were able, however, to prepare a single tryptophan actin mutant (W79) that had considerably reduced fluorescence emission compared with the wild-type F-actin. This would assist in the present studies to reduce the overall background signal, but it would not overcome the scattering artifact. The lack of any detectable change in signal from the actin tryptophans does not imply that actin does not change conformation during interaction with myosin (cf. 26), merely that this probe is not sensitive (or changes in individual residues cancel out).

As far as can be detected, actin has little or no direct effect on the fluorescence emission of W129 and W501. Previous work showed that actin binding to apo myosin to give a rigor complex was associated with little change in the lever arm position (27), and thus lack of perturbation of W501 is to be expected. Evidence for specific conformational changes induced by actin have been obtained at other locations. It is of interest to compare the present findings with the W129+ construct with our previous studies using a double cysteine mutant (S436C/N537C). Pyrene labeling of these cysteine residues allowed the movement of the actin-binding cleft to be monitored via changes in excimer fluorescence (21). A large amplitude fluorescence change was observed on formation of the actomyosin complex, and this was reversed on nucleotide-induced dissociation of actomyosin. We concluded that the cleft movement occurred prior to or coincident with nucleotide-induced actin dissociation. However, much smaller amplitudes were observed on nucleotide binding to the myosin construct in the absence of actin, suggesting the cleft was largely open in apo state of myosin. Structural studies indicate that cleft closure is coupled to switch 1 opening at the nucleotide site (28–30). The finding that the W129+ construct shows similar fluorescence amplitudes on nucleotide binding with and without actin suggests that this probe is not sensitive to rearrangements at the active site associated with switch 1 movements. We are now exploring other tryptophan substitutions in the active site, such as W239 in the switch 1 region, to define this relationship further (17).

Previous studies using tryptophan fluorescence revealed net changes on actomyosin interaction with other types of myosin. Johnson and Taylor (3) concluded there was a 14% enhancement in protein fluorescence when skeletal muscle subfragment 1 bound to actin in the absence of nucleotide, although the relative contributions from myosin and actin tryptophans could not be defined. From our results, it would appear that a myosin residue near the actin-binding interface (e.g., skeletal W595) is the likely source. Yengo et al. (31–33) have embarked on an extensive study of the actin binding interface of smooth muscle myosin and concluded that W546 (equivalent to *Dd* V534) showed a 10 nm blue shift on binding actin, while W625 (equivalent to *Dd* F612) was insensitive to actin binding. Mutations were made elsewhere in the actin-binding region of myosin and revealed that V413W (equivalent to *Dd* L404) showed a 3–9 nm red shift. The myosin cleft mutant F425W (equivalent to *Dd* S416) showed a fluorescence enhancement that paralleled actin binding and which was reversed in the presence of ATP. The latter study (33) was proposed to support the idea of cleft closure on actin binding. However, the measurements

were carried out in a stopped-flow apparatus using a WG320 cutoff filter (cf. Figure 3a), and therefore it would be of interest to determine magnitude of the fluorescence change compared with a tryptophanless myosin as a control, to assess the contribution from light scatter artifacts.

The effects of actin on nucleotide-induced changes in W501 fluorescence reveal details of the dissociation mechanism. Equation 2 represents the initial steps of the myosin ATPase (eq 1) expanded to include the equivalent actin-bound states.



Note the arrow length represents the approximate equilibrium position and the bold pathway shows the likely dominant route of dissociation of actin induced by ATP. From the signals reported by W129, located at the entrance to the nucleotide-binding site, we conclude actin has a minor effect ( $\leq 3$ -fold) on the forward rate constant for the isomerization step 2 (or its substeps 2a and 2b where resolved). This result is most clearly seen with ADP and ATP $\gamma$ S binding (Figures 5 and 6). With ATP itself, rapid dissociation of the actomyosin complex complicates the signal, but even here it is clear that step 2 is slowed by no more than 3-fold. W501, located at the distal end of the relay loop, also reports on the isomerization step 2 with a 10–20% quench, but with nucleoside triphosphates, the subsequent rapid step 3a usually nullifies the quench so that its kinetics cannot be resolved. ADP shows no tendency to undergo a reaction equivalent to step 3a, so that steps equivalent to 2 and 2' leading to the  $\dagger$ -state can be resolved and again show actin has only a 2-fold effect on this stage of the reaction (Figure 8).

The rapid dissociation of the  $A \cdot M^{\dagger} \cdot ATP$  complex prevented definition of the value of  $K'_{3a}$  with ATP as substrate. This problem was overcome by the use of ATP $\gamma$ S, because this substrate showed only slightly slower kinetics of binding and isomerization cf. ATP, but the rate of actomyosin dissociation is much reduced ( $k_c, k_d, k_e \approx 1 \text{ s}^{-1}$ ). Furthermore, because the ATP $\gamma$ S hydrolysis rate is slow, the early phase of the reaction reports on the  $K_{3a}$  equilibrium directly. Given the near correspondence between light scattering and cleft opening, as monitored by a pyrene excimer probe (21), it is expected that complex remains in the cleft-closed state, i.e., with strong binding to actin. In the absence of actin, the value of  $K_{3a}$  of 0.26 at 20 °C is close to that with ATP. In the presence of actin,  $K'_{3a}$  is 0.15 with ATP $\gamma$ S. By thermodynamic balance, it can be concluded actin binds to  $M^{\dagger} \cdot ATP\gamma$ S twice as tightly than  $M^* \cdot ATP\gamma$ S. Previous studies with other types of myosin have estimated the relative binding affinity of actin to myosins in different bound nucleotide states. Thus, Rosenfeld & Taylor (34) concluded that  $M \cdot ATP$  (i.e.,  $M^{\dagger} \cdot ATP/M^* \cdot ATP$  mixture) binds to actin about 3.5 times tighter than  $M^* \cdot ADP \cdot Pi$  with rabbit skeletal myosin at 20 °C.

Our measurements have implications for the mechanism of the reversal of the working stroke during muscle contraction. In the classic Lymn-Taylor (23) model, the repriming of the crossbridge stroke was depicted to occur after dissociation from actin. Subsequently, it was suggested that

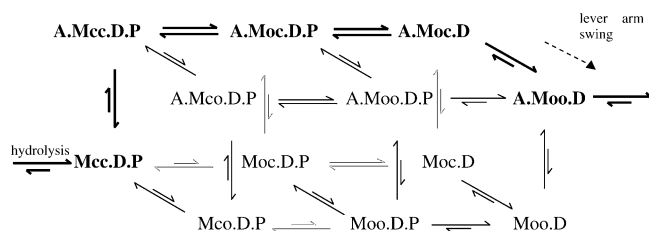


FIGURE 10: Kinetic scheme for actin activation of Pi and its coupling the lever arm swing. The status of the switch 1 and switch 2 are indicated by the first and second subscripts respectively (e.g., A·Moc·D·P has an open switch 1 and closed switch 2, T = ATP, D = ADP, P=Pi). The most likely pathway is shown in bold, assuming that switch 1 and switch 2 operate independently (see text for argument).

this step could occur prior to dissociation, provided the lifetime of the A·M·ATP state was very short so that it made little contribution to net force in an ensemble of crossbridges (35). Recent optical trap studies have attempted to address this issue by investigating whether actomyosin bond formation is intrinsically coupled to a power stroke and whether dissociation of this state by non- or slowly hydrolysable analogues leads to a reverse stroke (36, 37). These studies led to the conclusion that there was no discernible stroke (to within 1 nm) with ATP $\gamma$ S compared with the 5 nm stroke estimated for ATP itself. The lack of a measurable displacement is in accord with our own data which suggest that, at 20 °C, 20% of the actin-free myosin motors are in the M<sup>\*</sup>·ATP $\gamma$ S state, but these may only contribute to 10% of the observed events because of the 2-fold selectivity in binding to the open state (i.e., 90% of the dissociation events go via route c compared with d in eq 2). Thus, the expected mean displacement in the optical trap would be 0.5 nm, which is just below the detection limit.

Our findings also have implications for actin-activation of the product-release steps. Figure 10 shows a general model for phosphate release as a result of opening switch 1 and switch 2. The status of the switches is indicated by the subscripts o and c. We assume that the quenched fluorescence state, M<sup>†</sup> is indicative of an open switch 2, while the enhanced fluorescence state M<sup>\*</sup> is indicative of a closed switch 2. However, the status of switch 1 is not defined by the fluorescence of W129 nor W501. If we assume that actin has little or no effect on the rate and equilibrium constants of the switch 2 open-closed transition (as we observe for the nucleoside triphosphate complex), how does actin activate Pi release? The kinetics of the M<sup>\*</sup>·ADP·Pi  $\leftrightarrow$  M<sup>†</sup>·ADP·Pi transition (i.e., Mcc·D·P  $\leftrightarrow$  Mco·DP in Figure 10) are not fully defined (11). If the transition is rapid compared with subsequent steps then the equilibrium must lie to the left because M<sup>\*</sup>·ADP·Pi is the predominant steady-state intermediate. Even if the reaction is slow, then there is still evidence that the reaction is poised to the left, or at least is not strongly poised to the right, because significant equilibrium concentrations (25% total M) of M<sup>\*</sup>·ADP·Pi can be synthesized by adding subsaturating (25 mM) concentrations of Pi to M<sup>†</sup>·ADP (11). The value at saturating Pi concentrations is difficult to determine because of the influence of the ionic strength. Nevertheless, the equilibrium position is sufficiently well defined to conclude that the corresponding equilibrium constant for the actin-bound states (A·Mcc·D·P  $\leftrightarrow$  A·Mco·DP) cannot lie strongly to the right either. This transition, although accompanied by a lever arm swing, is

unlikely to provide an effective working stroke on the grounds that (1) A·Mcc·D·P and A·Mco·DP are weakly bound states that rapidly dissociate from actin and thus could not bear tension. (2) The reaction would need to be “pulled” by the subsequent Pi-release step to make it energetically favorable, which gives a potential problem with futile cycling (i.e., via Mcc·D·P  $\leftrightarrow$  Mco·DP  $\leftrightarrow$  A·Mco·DP), unless the kinetics of actin-bound pathway are somehow selectively accelerated. What alternative route exists?

Structural studies indicate that strong actin binding results from closure of the 50K cleft and concomitant opening of switch 1 (28–30). There is also kinetic evidence for such coupling in that actin binding affects the rate and/or amplitude of fluorescence signals arising from cleft probes (21), as well as tryptophan residues within the switch 1 loop (17). We propose that, following actin binding, switch 1 opens before switch 2 and therefore A·Mcc·D·P  $\leftrightarrow$  A·Moc·D·P is the preferred route in Figure 10. A·Moc·D·P has a high affinity for actin because cleft closure gives increased contacts, but the equilibrium constant A·Moc·D·P  $\leftrightarrow$  A·Moo·D·P remains similar to that for the Mcc·D·P  $\leftrightarrow$  Mco·D·P transition (on the grounds that the K<sub>3a</sub> equilibrium constant for the M.ATP $\gamma$ S complex is practically independent of whether actin is strongly bound or not). Similarly, the A·Moc·D·P  $\leftrightarrow$  A·Moo·D·P transition is unlikely to produce an effective working stroke for the second reason alluded to above. Provided Pi can escape on switch 1 opening, then the preferred route to A·Moo·D would be via A·Moc·D, i.e., Pi release occurs before the lever arm swing associated with switch 2 opening. It is known that the Moc·D  $\leftrightarrow$  Moo·D equilibrium (i.e., M<sup>\*</sup>·ADP  $\leftrightarrow$  M<sup>†</sup>·ADP) lies strongly to the right (6) and therefore the equivalent A·Moc·D  $\leftrightarrow$  A·Moo·D will share this property and have sufficient energy to drive the working stroke. If, on the other hand, Pi cannot escape until switch 2 opens as well, then the lever arm swing associated with the relatively unfavorable A·Moc·D·P  $\leftrightarrow$  A·Moo·D·P transition will require the subsequent Pi release step to “pull” the equilibrium over. The first route (i.e., Pi release prior to lever arm movement) has the advantage that the relatively irreversible Pi release step (at physiological Pi concentrations of < 1 mM) results in a commitment that minimizes futile cycling.

What support can be offered for the route via A·Moc·D with Pi release preceding the working stroke at physiological Pi concentrations? The A·Moc·ADP state cannot be generated by addition of ADP to A·Moo to any significant degree. This property is shared by the so-called Sleep-Hutton AM'-ADP state (38), which exists at detectable concentrations only during the steady-state turnover of ATP. This state was proposed on the basis of the ATP  $\leftrightarrow$  Pi exchange kinetics during ATP turnover by skeletal muscle myosin being about 50 times faster than expected for Pi binding to the A·M·ADP state formed at equilibrium. Moreover, the scheme of Figure 10 requires that the A·Moc·D state must bind Pi more tightly than the predominant state at equilibrium (A·Moo·D) to account for the change in the switch 2 equilibrium constant from being unfavorable (or at most weakly favorable) in the A·Moc·D·P  $\leftrightarrow$  A·Moo·D·P transition to being strongly favorable in the A·Moc·D  $\leftrightarrow$  A·Moo·D transition. This makes structural sense in that the Pi would be stabilized by interaction with the closed switch 2. Furthermore, if the lever arm movement is restrained, as in an isometric muscle,

the A·Moc·D state would be more favored, leading to the potential for increased ATP ↔ Pi exchange in organized systems compared with proteins in solution, as is observed (38). Our assumption that actin has little effect on the switch 2 equilibrium constant requires the A·Moc·D and A·Moo·D states to have similar affinities for actin, and the latter is known to be relatively tight binding. Thus, A·Moc·D would likely dissociate from actin slowly, which is important to prevent the futile cycle that would result from the A·Moc·D ↔ Moc·D ↔ Moo·D route. Taylor (39) identified a minor A·M·ADP species (denoted A\*·M·D) which had a relatively fast dissociation rate and he equated this species with the Sleep-Hutton AM'-ADP state (38). However, apart from its equilibrium concentration being in the correct range, there is no direct evidence for this assignment. The Taylor A\*·M·D state has enhanced actin-pyrene fluorescence and hence presumably is a weak binding state with an open cleft. As discussed by Steffen & Sleep (37), the reported properties of the Taylor A\*·M·D state (39) would lead to inefficient coupling owing to rapid actin dissociation.

Recently, Rosenfeld & Sweeney (40) have characterized the myosin V ATPase mechanism and concluded that the working stroke occurs after Pi release. They proposed that actin-activated Pi release is the primary step following actin binding and that Pi release occurs via switch 1 opening, as evidenced by the coincidence of the signal from the Pi binding protein sensor and the change in methylantraniloyl nucleotide fluorescence. The latter appears to act as a probe of switch 1 movement because the methylantraniloyl fluorophore lies on the protein surface close to switch 1 (41). Indeed, many years earlier, Woodward et al. (42) concluded that the strong binding of actin to myosin II was associated with a global conformation change in myosin owing to the coincidence of the pyrene actin and methylantraniloyl nucleotide signals. Modeling the actomyosin complex from crystal structures (28–30) subsequently revealed these sites to be located about 5.6 nm apart. The myosin V mechanism proposed by Rosenfeld & Sweeney (40) shares a key feature with our proposed scheme for *Dd* myosin II, that Pi can escape without the need for switch 2 opening. However, the ADP release steps of myosin V are somewhat modified to give a high duty motor with additional lever arm movement.

Many experiments on the effects of phosphate on tension transients in muscle have led to models in which the crossbridge stroke precedes Pi release (43–47). Interestingly, for a feasible set of rate constants to describe the two routes of decay of A·Moc·D·P to A·Moo·D in Figure 10, the flux can be made to switch from the A·Moc·D route at low Pi (i.e., < 5 mM, the  $K_d$  assigned to the A·Moc·D·P complex) to the A·Moo·D·P route at high Pi (i.e., >250 mM, the  $K_d$  assigned to the A·Moo·D complex). In a muscle the fluxes are more difficult to calculate because of the strain dependence of the rate constants confound this issue further, and tension changes can arise from redistributions of a disproportionately small population of crossbridges. Nevertheless, the above modeling indicates that the preferential route can change depending on conditions.

The apparent discrepancy with the physiological data could also arise if the working stroke arose from transitions other than those associated with opening of switch 2. Tension generation before Pi release could occur if the crossbridge stroke (or at least part of it) arose from rotation of the whole

motor domain such as that associated with the weak (disordered) to strong (stereospecific) binding of actin (48, 49). It is likely that W501 fluorescence is insensitive to such rearrangements at the actin-binding interface, and therefore our data neither support nor exclude this kind of mechanism. However, recently Holmes et al. (8) suggested that actin binding is directly coupled to lever arm movement without the need for switch 2 opening. This proposal was based on the crystal structure of myosin V, which shows the 50K domain cleft is closed in its apo state (29), as predicted for the structure for myosin II when bound to actin in a high affinity (rigor-like) state (28). Cleft closure is accompanied by a twisting of the central  $\beta$  sheet, and this relieves the potential steric clash with the relay helix, and so uncouples the switch 2 movement from the lever arm swing (8). Thus, in the closed-cleft (rigor-like) state, the lever-arm is in the post-power stroke (down) state, while switch 2 remains closed. The structure leads to a new idea for coupling to mechanics in that when M\*·ADP·Pi (switch 2 closed, relay loop kinked) binds to actin, the subsequent cleft closure increases the affinity to actin and, concomitantly, the  $\beta$ -strand movement allows the relay loop to unkink, so allowing the lever arm to swing back to the post-power stroke state (cf. the earlier idea (5) that the power stroke involved the lever arm movement accompanying the opening of switch 2). Thus, in the scheme of Figure 10, the lever arm swing would accompany the A·Mcc·D·P ↔ A·Moc·D·P transition. This mechanism would also allow ATP to dissociate the actomyosin rigor complex without any change to the lever arm position from its post-power stroke position.

The Holmes et al. (8) model has implications for our interpretation of W501 fluorescence because the latter cannot be assumed to report on the position of the switch 2 loop in actin-bound states, as we have done previously for myosin states. Rather, it seems more accurate to relate W501 fluorescence to the position of the lever arm because W501 is located distal to the kink induced in the relay loop (Figure 1). Regardless, our data indicate that when the myosin motor is bound to actin in the presence of nucleoside triphosphate (i.e., a ternary complex), the W501 fluorescence is intermediate between the extreme † and \* states, as a result of rapid exchange between them, with an equilibrium constant only 2-fold lower than that observed in the absence of actin. The Holmes et al. (8) model would predict that the lever arm would show much less tendency to occupy the prepower stroke state when the myosin is strongly bound to actin in the bound ATP state. The expected W501 fluorescence transient on mixing A·M with ATP $\gamma$ S at 20 °C would therefore show a quench phase as seen at 2 °C (Figure 9a). This is not observed. Thus, there is no support from our data that the status of the cleft and switch 1 has any marked effect on the position of the lever arm, as sensed by W501. This has yet to be tested directly for the case quaternary complexes of actin with the myosin-ADP·Pi intermediate.

## ACKNOWLEDGMENT

We thank Professor Ken Holmes for stimulating discussions.

## REFERENCES

1. Bagshaw, C. R., and Trentham, D. R. (1974) The characterization of myosin-product complexes and of product-release steps during

- the magnesium ion-dependent adenosine triphosphatase reaction, *Biochem. J.* 141, 331–349.
2. Bagshaw, C. R., Eccleston, J. F., Eckstein, F., Goody, R. S., Gutfreund, H., and Trentham, D. R. (1974) The magnesium ion-dependent adenosine triphosphatase of myosin. Two-step processes of adenosine triphosphate association and adenosine diphosphate dissociation, *Biochem. J.* 141, 351–364.
  3. Johnson, K. A., and Taylor, E. W. (1978) Intermediate states of subfragment 1 and actosubfragment 1 ATPase: reevaluation of the mechanism, *Biochemistry* 17, 3432–3442.
  4. Millar, N. C., and Geeves, M. A. (1988) Protein fluorescence changes associated with ATP and adenosine 5'-[gamma-thio]-triphosphate binding to skeletal muscle myosin subfragment 1 and actomyosin subfragment 1, *Biochem. J.* 249, 735–743.
  5. Geeves, M. A., and Holmes, K. C. (1999) Structural mechanism of muscle contraction, *Annu. Rev. Biochem.* 68, 687–728.
  6. Malnasi-Csizmadia, A., Pearson, D. S., Kovacs, M., Woolley, R. J., Geeves, M. A., and Bagshaw, C. R. (2001) Kinetic resolution of a conformational transition and the ATP hydrolysis step using relaxation methods with a Dictyostelium myosin II mutant containing a single tryptophan residue, *Biochemistry* 40, 12727–12737.
  7. Fisher, A. J., Smith, C. A., Thoden, J. B., Smith, R., Sutoh, K., Holden, H. M., and Rayment, I. (1995) X-ray structures of the myosin motor domain of Dictyostelium discoideum complexed with MgADP.BeFx and MgADP. AIF<sub>4</sub>, *Biochemistry* 34, 8960–8972.
  8. Holmes, K. C., Schroder, R. R., Eschenburg, S., Sweeney, H. L., and Houdusse, A. (2004) The structure of the rigor complex and its implications for the power stroke, *Philos. Trans. R. Soc. London B Biol. Sci.*, in press.
  9. Shih, W. M., and Spudich, J. A. (2001) The myosin relay helix to converter interface remains intact throughout the actomyosin ATPase cycle, *J. Biol. Chem.* 276, 19491–19494.
  10. Malnasi-Csizmadia, A., Woolley, R. J., and Bagshaw, C. R. (2000) Resolution of conformational states of Dictyostelium myosin II motor domain using tryptophan (W501) mutants: Implications for the open-closed transition identified by crystallography, *Biochemistry* 39, 16135–16146.
  11. Wakelin, S., Conibear, P. B., Woolley, R. J., Floyd, D. N., Bagshaw, C. R., Kovacs, M., and Malnasi-Csizmadia, A. (2002) Engineering Dictyostelium discoideum myosin II for the introduction of site-specific probes, *J. Muscle Res. Cell Motil.* 24, 673–683.
  12. Bagshaw, C. R., Eccleston, J. F., Trentham, D. R., Yates, D. W., and Goody, R. S. (1972) Transient kinetic studies of the Mg<sup>2+</sup>-dependent ATPase of myosin and its proteolytic subfragments, *Cold Spring Harbor Symp. Quant. Biol.* 37, 127–135.
  13. Werber, M. M., Szent-Gyorgyi, A. G., and Fasman, G. D. (1972) Fluorescence studies on heavy meromyosin-substrate interaction, *Biochemistry* 11, 2872–2883.
  14. Urbanke, C., and Wray, J. (2001) A fluorescence temperature-jump study of conformational transitions in myosin subfragment 1, *Biochem. J.* 358, 165–173.
  15. Holmes, K. C., and Geeves, M. A. (2000) The structural basis of muscle contraction, *Philos. Trans. R. Soc. London B Biol. Sci.* 355, 419–431.
  16. Bagshaw, C. R., and Trentham, D. R. (1973) The reversibility of adenosine triphosphate cleavage by myosin, *Biochem. J.* 133, 323–328.
  17. Zeng, W., Conibear, P. B., Dickens, J. L., Cowie, R. A., Wakelin, S., Malnasi-Csizmadia, A., and Bagshaw, C. R. (2004) Dynamics of actomyosin interactions in relation to the crossbridge cycle, *Philos. Trans. R. Soc. London B Biol. Sci.*, in press.
  18. Kovacs, M., Malnasi-Csizmadia, A., Woolley, R. J., and Bagshaw, C. R. (2002) Analysis of Nucleotide Binding to Dictyostelium Myosin II Motor Domains Containing a Single Tryptophan Near the Active Site, *J. Biol. Chem.* 277, 28459–28467.
  19. Spudich, J. A., and Watt, S. (1971) The regulation of rabbit skeletal muscle contraction. I. Biochemical studies of the interaction of the tropomyosin-troponin complex with actin and the proteolytic fragments of myosin, *J. Biol. Chem.* 246, 4866–4871.
  20. Lakowicz, J. R. (1999) *Principles of Fluorescence Spectroscopy*, 2nd ed., Kluwer Academic/Plenum Press, New York.
  21. Conibear, P. B., Bagshaw, C. R., Fajer, P. G., Kovacs, M., and Malnasi-Csizmadia, A. (2003) Myosin cleft movement and its coupling to actomyosin dissociation, *Nat. Struct. Biol.* 10, 831–835.
  22. Kuhlman, P. A., and Bagshaw, C. R. (1998) ATPase kinetics of the Dictyostelium discoideum myosin II motor domain, *J. Muscle Res. Cell Motil.* 19, 491–504.
  23. Lynn, R. W., and Taylor, E. W. (1971) Mechanism of adenosine triphosphate hydrolysis by actomyosin, *Biochemistry* 10, 4617–4624.
  24. Webb, M. R., and Trentham, D. R. (1980) The stereochemical course of phosphoric residue transfer during the myosin ATPase reaction, *J. Biol. Chem.* 255, 8629–8632.
  25. Doyle, T. C., Hansen, J. E., and Reisler, E. (2001) Tryptophan fluorescence of yeast actin resolved via conserved mutations, *Biophys. J.* 80, 427–434.
  26. Prochniewicz, E., Walseth, T. F., and Thomas, D. D. (2004) Structural dynamics of actin during active interaction with myosin: different effects of weakly and strongly bound myosin heads, *Biochemistry* 43, in press.
  27. Xiao, M., Reifengerger, J. G., Wells, A. L., Baldacchino, C., Chen, L. Q., Ge, P., Sweeney, H. L., and Selvin, P. R. (2003) An actin-dependent conformational change in myosin, *Nat. Struct. Biol.* 10, 402–408.
  28. Holmes, K. C., Angert, I., Kull, F. J., Jahn, W., and Schroder, R. R. (2003) Electron cryo-microscopy shows how strong binding of myosin to actin releases nucleotide, *Nature* 425, 423–427.
  29. Coureux, P. D., Wells, A. L., Menetrey, J., Yengo, C. M., Morris, C. A., Sweeney, H. L., and Houdusse, A. (2003) A structural state of the myosin V motor without bound nucleotide, *Nature* 425, 419–423.
  30. Reubold, T. F., Eschenburg, S., Becker, A., Kull, F. J., and Manstein, D. J. (2003) A structural model for actin-induced nucleotide release in myosin, *Nat. Struct. Biol.* 10, 826–830.
  31. Yengo, C. M., Fagnant, P. M., Chrin, L., Rovner, A. S., and Berger, C. L. (1998) Smooth muscle myosin mutants containing a single tryptophan reveal molecular interactions at the actin-binding interface, *Proc. Natl. Acad. Sci. U.S.A.* 95, 12944–12949.
  32. Yengo, C. M., Chrin, L., Rovner, A. S., and Berger, C. L. (1999) Intrinsic tryptophan fluorescence identifies specific conformational changes at the actomyosin interface upon actin binding and ADP release, *Biochemistry* 38, 14515–14523.
  33. Yengo, C. M., De La Cruz, E. M., Chrin, L. R., Gaffney, D. P., 2nd, and Berger, C. L. (2002) Actin-induced closure of the actin-binding cleft of smooth muscle myosin, *J. Biol. Chem.* 277, 24114–24119.
  34. Rosenfeld, S. S., and Taylor, E. W. (1984) The ATPase mechanism of skeletal and smooth muscle actin-subfragment 1, *J. Biol. Chem.* 259, 11908–11919.
  35. Eisenberg, E., and Greene, L. E. (1980) The relation of muscle biochemistry to muscle physiology, *Annu. Rev. Physiol.* 42, 293–309.
  36. Steffen, W., Smith, D., and Sleep, J. (2003) The working stroke upon myosin-nucleotide complexes binding to actin, *Proc. Natl. Acad. Sci. U.S.A.* 100, 6434–6439.
  37. Steffen, W., and Sleep, J. (2004) Using optical tweezers to relate the chemical and mechanical crossbridge cycles, *Philos. Trans. R. Soc. London B Biol. Sci.*, in press.
  38. Sleep, J. A., and Hutton, R. L. (1980) Exchange between inorganic phosphate and adenosine 5'-triphosphate in the medium by actomyosin subfragment 1, *Biochemistry* 19, 1276–1283.
  39. Taylor, E. W. (1991) Kinetic studies on the association and dissociation of myosin subfragment 1 and actin, *J. Biol. Chem.* 266, 294–302.
  40. Rosenfeld, S. S., and Sweeney, H. L. (2004) A Model of Myosin V Processivity, *J. Biol. Chem.* 279, 40100–40111.
  41. Bauer, C. B., Kuhlman, P. A., Bagshaw, C. R., and Rayment, I. (1997) X-ray crystal structure and solution fluorescence characterization of Mg 2'(3')-O-(N-methylanthraniloyl) nucleotides bound to the Dictyostelium discoideum myosin motor domain, *J. Mol. Biol.* 274, 394–407.
  42. Woodward, S. K., Eccleston, J. F., and Geeves, M. A. (1991) Kinetics of the interaction of 2'(3')-O-(N-methylanthraniloyl)-ATP with myosin subfragment 1 and actomyosin subfragment 1: characterization of two acto-S1-ADP complexes, *Biochemistry* 30, 422–430.
  43. Fortune, N. S., Geeves, M. A., and Ranatunga, K. W. (1991) Tension responses to rapid pressure release in glycerinated rabbit muscle fibers, *Proc. Natl. Acad. Sci. U.S.A.* 88, 7323–7327.
  44. Dantzig, J. A., Goldman, Y. E., Millar, N. C., Lactis, J., and Homsher, E. (1992) Reversal of the cross-bridge force-generating transition by photogeneration of phosphate in rabbit psoas muscle fibres, *J. Physiol.* 451, 247–278.

45. Wang, G., and Kawai, M. (1997) Force generation and phosphate release steps in skinned rabbit soleus slow-twitch muscle fibers, *Biophys. J.* 73, 878–894.
46. Ranatunga, K. W., Coupland, M. E., and Mutungi, G. (2002) An asymmetry in the phosphate dependence of tension transients induced by length perturbation in mammalian (rabbit psoas) muscle fibres, *J. Physiol.* 542, 899–910.
47. Smith, D. A., and Sleep, J. (2004) Mechanokinetics of rapid tension recovery in muscle: the Myosin working stroke is followed by a slower release of phosphate, *Biophys. J.* 87, 442–456.
48. Thomas, D. D., Ramachandran, S., Roopnarine, O., Hayden, D. W., and Ostap, E. M. (1995) The mechanism of force generation in myosin: a disorder-to-order transition, coupled to internal structural changes, *Biophys. J.* 68, 135S–141S.
49. Bershtitsky, S. Y., Tsaturyan, A. K., Bershtitskaya, O. N., Mashanov, G. I., Brown, P., Burns, R., and Ferenczi, M. A. (1997) Muscle force is generated by myosin heads stereospecifically attached to actin, *Nature* 388, 186–190.
50. Smith, C. A., and Rayment, I. (1996) X-ray structure of the magnesium(II).ADP.vanadate complex of the Dictyostelium discoideum myosin motor domain to 1.9 Å resolution, *Biochemistry* 35, 5404–5417.

BI048338J